ACS Energy LETTERS

http://pubs.acs.org/journal/aelccp

LETTER

The Impact of Piezoelectricity in Low Dimensional Metal Halide Perovskite

Stav Rahmany, Adva Shpatz Dayan, Małgorzata Wierzbowska, Amanda Jiamin Ong, Yun Li, Shlomo Magdassi, Alfred Iing Yoong Tok, and Lioz Etgar*

Cite This: *ACS Energy Lett.* 2024, 9, 1527−1536

Read Online

ACCESS | Metrics & More | Article Recommendations | Supporting Information

ABSTRACT: **Hybrid perovskites show piezoelectric properties due to polarization and centro-symmetry breaking of PbX_6 pyramids (X = I-, Br-, Cl-). This study examines the piezoelectric response of quasi-2D perovskites using various barrier molecules: benzyl amine (BzA), phenylethyl amine (PEA), and butyl diamine (BuDA). Utilizing piezoelectric force microscopy measurements, we determine the piezoelectric coefficient (d_{33}) where BuDA exhibits a substantial response with values of 147 pm V^{-1} for n = 5, better than the other quasi-2D and 3D perovskite counterparts. Density functional theory calculations reveal distorted bond angles in the $PbBr_6$ pyramids for quasi-2D perovskites, enhancing symmetry breaking. Additionally, polarizabilities and dielectric constants, derived from *ab initio* many-body perturbation theory, are highest for BuDA, followed by PEA and BzA, aligning with experimental results. We demonstrate pressure sensor performance, emphasizing the quicker capacitance decay time of the quasi-2D perovskite based on BuDA. This research underscores the impact of perovskite dimensionality on piezoelectricity, paving the way for the development of sensitive and wide-ranging pressure sensors.**

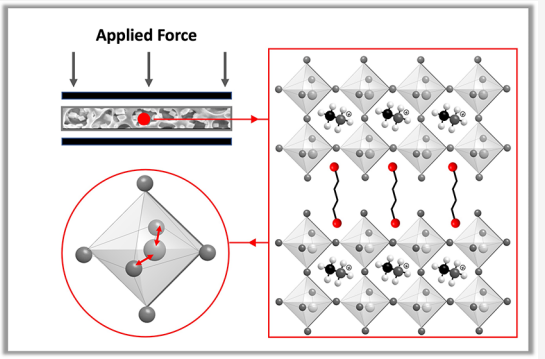

Halide perovskite is considered an excellent candidate for third generation photovoltaics (PV) due to its unique optical and physical properties. Halide perovskites have a general structure of ABX_3 in which A is an organic or inorganic monovalent cation (Cs^+, Rb^+, MA^+, or FA^+), B is a divalent metal cation with a coordination number of 6 (e.g., Pb^{2+} or Sn^{2+}), and X is a halide anion (I^-, Br^-, Cl^-) which binds with the metallic cation to form BX_6 octahedral sheets where the A-site cation lays within the octahedral holes.[1−6] The radii of the A-site cation have a significant influence on the formed structure according to the Goldschmidt tolerance factor; in order to form a three-dimensional (3D) structure with continuous BX_6 sheets along the entire crystal lattice, the value of the factor should be in the range of $0.8 < t < 1.1$.[7−10] Incorporation of a larger radius A-site organic cation (R corresponds to barrier molecule) will cause a separation between the BX_6 octahedral sheets along the Z axis forming the $R_2A_{n-1}B_nX_{3n+1}$ formula with a quasi-two-dimensional (2D) ($n \geq 1$) perovskite structure.[11] Unlike 3D perovskites in which the optical properties are controlled mainly by the B−X orbitals overlap, in the quasi-2D structure, in addition to the halide type, the optical and electronic properties of the material are significantly influenced by the size and chemical structure of the R cation as a result of quantum confinement effects. The quasi-2D perovskite can be divided into two subcategories: (i) Dion-Jacobson (DJ) in which there is a single R cation molecule containing two amine groups at the opposite ends and (ii) Ruddlesden−Popper (RP) which is composed of two monoamine R cations oriented in the opposite directions.[12−14] Recent studies have shown that the quasi-2D structure is more stable compared to the 3D perovskite under humidity conditions.[15−17] Along with its excellent solar energy harvesting properties, halide perovskites also demonstrate piezoelectric energy harvesting.[18−20] In the piezoelectric device, the charge density (q_3) generated as a response to an applied uniaxial pressure (σ_z) that acts on the surface area (A) derives from the changes in the electric displacement (e_3) inside the material, i.e., $q_3 = e_3 dA$. Further, it is related to the piezoelectric coefficient (d_{33}) and the macroscopic dielectric constant across the structure (ε_{33} or ε_r, so-called relative permittivity $\varepsilon/\varepsilon_0$ with respect to the vacuum permittivity ε_0) via the formula $e_3 = d_{33}\,\sigma_z + \varepsilon_{33}E_3$, where E_3 is the electric field component along the pressure

Received: January 17, 2024
Revised: February 10, 2024
Accepted: February 21, 2024
Published: March 14, 2024

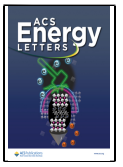

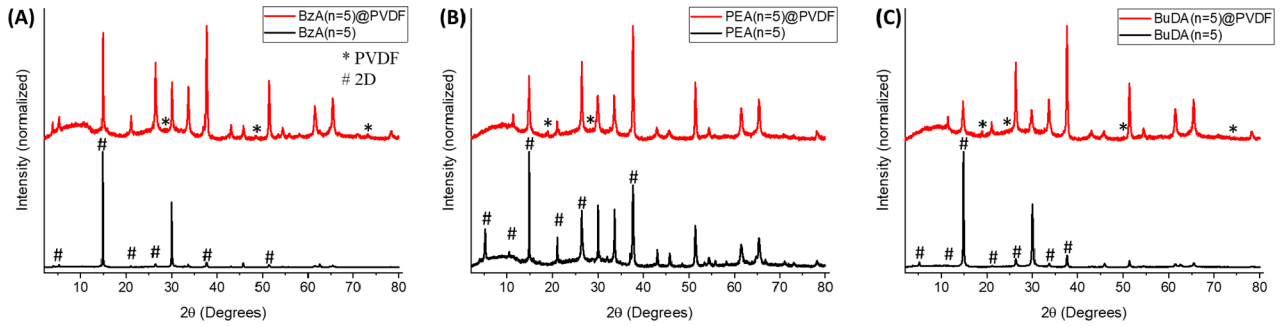

Figure 1. X-ray diffraction patterns for 2D (n = 5) perovskite composition based on (A) benzyl amine, (B) phenylethyl amine, and (C) butyl diamine with (red) and without (black) PVDF.

axis. On the other hand, the electric displacement and polarization of the material (P_z) are related via $e_3 = P_z + \varepsilon_0 E_3$. Since the piezoelectric effect is formed due to mechanical stress, it strongly depends on the perovskite components, as those affect the lattice structure.

Inorganic $CsPbBr_3$ perovskite is theoretically estimated to have a polarization of 0.45 μC cm^{-2} which could be enlarged to 23 μC cm^{-2} under mechanical stress due to lattice distortion.[21] A large polarization value of 63 μC cm^{-2} was observed for $FAPbI_3$ composition as a result of the large cation size which induces polar deformations in the PbI_3 cage.[22] The $MAPbI_3$-based piezoelectric energy-harvesting devices exhibit an output piezoelectric effect of 2.7 V and 140 nA cm^{-2}. The effective piezoelectric coefficient (d_{33}) of this composition was found to be in the range of 6 to 25 pm V^{-1} using piezoelectric force microscopy (PFM).[23] The piezoelectric phenomena were proven by Bu and co-workers to exist also in 2D perovskites. Their study on chiral 2D perovskite using R/S-$[BPEA]_2PbI_4$ yielded voltages and currents of 0.6 V and 1.5 μA under an applied force of 2N.[24] In order to further enhance the piezoelectric effect in pressure sensor devices, halide perovskites were used as filler materials in PVDF (polyvinylidene fluoride) polymers, forming a perovskite−PVDF composite.[25−27] The $MAPbI_3$−PVDF composite showed an increase in the dielectric constant of ε_r (∼56) compared to pure PVDF film (∼12.6).[26] The same effect was demonstrated in $MASnBr_3$−PDMS (polydimethylsiloxane) composite in which the value of ε_r was nearly ten-times larger than that of PDMS (36.2 compared to 3.2).[28]

Herein, we performed a comprehensive study of the piezoelectric response in quasi-2D perovskites based on different barrier molecules. We focused on three barrier molecules, benzyl amine (BzA), phenylethyl amine (PEA), and butyl diamine (BuDA), which were incorporated in the perovskite having the chemical formula $R_2MA_{n-1}Pb_nBr_{3n+1}$. The A-site cation in the perovskite structure influences the distance between the BX_6 octahedral sheets. As a result, it directly impacts the ability of the material to contract under an applied external field. Hence, the nature of the barrier molecules in terms of their length, functional groups, and linear or aromatic structure affects the piezoelectric properties. Motivated by the above reasons, we performed a series of piezoelectric force microscopy (PFM) measurements and studied the piezoelectric response of each composition by analyzing the effect of the barrier molecule over the piezoelectric properties. In addition, we conducted a series of theoretical calculations to understand the structural changes of each composition under an applied pressure as a function of the barrier molecule which supports the observed enhancement of the piezoelectric effect in the 2D perovskite.

Our study focuses on quasi-2D perovskites based on methylammonium (MA) bromide with the addition of different barrier molecules. We used a linear barrier (BuDABr = butyl diamine bromide) with two amine groups, an aromatic barrier with a short-chain residue (BzABr = benzyl amine bromide), and an aromatic barrier containing an additional carbon in the chain residue (PEABr = phenylethylammonium bromide). Using each barrier, we prepared a solution of quasi-2D perovskite with the composition of $R_2MA_{n-1}Pb_nBr_{3n+1}$ where n = 1, n = 5, n = 10 and n = 50 while using a 3D composition of $MAPbBr_3$ as a reference experiment. Each perovskite composition was mixed with polyvinylidene fluoride (PVDF) to form perovskite:PVDF composite in a ratio of 25:75 based on earlier reports.[23] PVDF is known as a piezoelectric polymer and its role is to enhance the piezoelectric response of the perovskite material.[26,27,29]

Each composition was deposited by spin coating to form a continuous, uniform film. In order to see the PVDF incorporation and morphology, we performed scanning electron microscopy (SEM) of the composite films. Figure S1A−C show the morphology of the neat BzA-, PEA-, and BuDA-based quasi-2D perovskites with n = 5, respectively. It can be seen that the quasi-2D perovskite forms a multicrystalline cubic shape. The same compositions with the addition of PVDF are presented in Figure S1D−F. As shown, PVDF formed a typical web structure where the perovskite crystals lay within it. The crystal structure shape remains unchanged upon mixing with PVDF. However, there is a reduction in the crystal size for the BzA- and PEA-based perovskites. The BzA crystals' average size reduced from 0.58 ± 0.07 μm to 0.32 ± 0.06 μm, while the corresponding reduction for PEA was from 0.25 ± 0.09 μm to 0.21 ± 0.07 μm. The changes in the crystal size derive from the size growth limitation due to the presence of PVDF which is bulky and prevents the natural growth of the perovskite crystals. Next, we study the crystallographic structure of both neat perovskite and perovskite:PVDF films by X-ray diffraction (XRD) measurements. Figure 1 shows the XRD spectra for all three quasi-2D perovskite compositions based on the different barriers, with (red plot) and without (black plot) PVDF. For all three barriers, the main crystallographic peak of the perovskite at 14.8°, 26.4°, and 37.6° remained after mixing with PVDF. All barriers compositions before the PVDF incorporation show the 2D peak at 5.2° (plane 002). It can be seen that in the case of PEA- (Figure 1B) and BuDA- (Figure 1C) based perovskites, the main peak disappears upon mixing with PVDF. It can be related to a

https://doi.org/10.1021/acsenergylett.4c00177
ACS Energy Lett. 2024, 9, 1527−1536

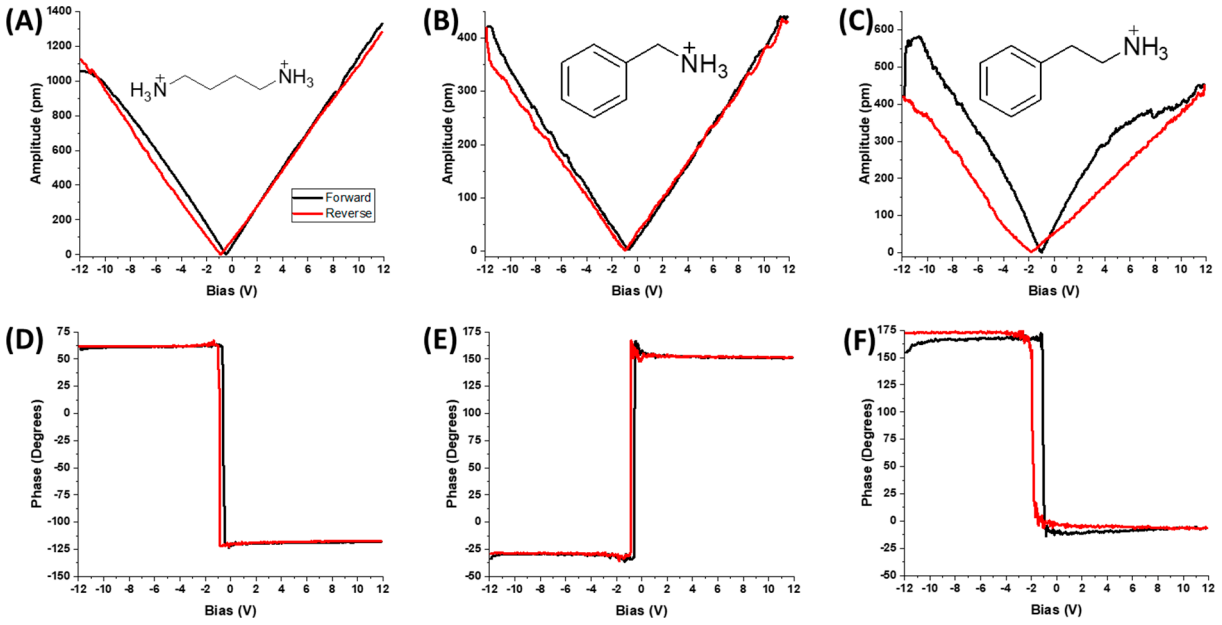

Figure 2. Local piezoelectric measurements (horizontal) for n = 1 perovskite based on (A) butyl diamine, (B) benzyl amine, and (C) phenylethyl amine barriers in the solution with 75% PVDF. The drawing shows a schematic illustration of each barrier molecule. The corresponding phase curves were measured for the compositions with (D) BuDA, (E) BzA, and (F) PEA.

shielding effect created by the PVDF in those regions. However, the peak at 11.4° (plane 004), which is also related to 2D perovskite, becomes more dominant compared to the neat perovskite films for PEA- and BuDA-based perovskites.

Apparently, not only do the perovskite crystals get smaller when growing inside the PVDF matrix but also the preferred growth planes are changing. Quasi-2D perovskites with $n > 1$ are composed from a mixture of several "n" values in the same film as was also reported earlier in the literature.[30−32] The quasi-2D related peaks at 26.4° (plane 0010) and 37.6° (plane 0014) increase their intensity and become the dominant peaks. Hence, it can be assumed that PVDF also enhances the growth of the quasi-2D phase in the mixture of 3D and quasi-2D perovskite. One of the key features in piezoelectric materials is the lack of symmetry. In perovskite, the symmetry breaking derives from a movement of the b-site cation from the center of the octahedron as a result to an applied external pressure. This movement is responsible for the dipole formation which contributes to the piezoelectric response in halide perovskite. In order to understand the initial symmetry (before external pressure was applied), we grow single crystal (SC) of the pure 2D (n = 1) based on each barrier molecule and performed single crystal (SC) XRD analysis in order to obtain the space group for each composition. The space group can give us an indication regarding the symmetry of the system in its initial state. The analyzed data of PEA-, BzA-, and BuDA-based SC XRD can be found in Figures S2−S4, respectively. It was found that PEA- and BuDA-based 2D perovskites are triclinic systems and have a space group of *P-1* without any mirror plane or rotation, and the lack of inversion center makes those two systems nonsymmetric. The BzA composition shows that a *Cmce* space group belongs to the monoclinic crystal system. In this structure, there is a rotation axis and a mirror plane, and therefore, it is considered symmetric. However, in the case of metal halide perovskite, there is a local symmetry breaking due to structural distortions that occur in the crystallization process or formed upon external pressure which changes the system symmetry.

Absorbance measurements for each PVDF:quasi-2D perovskite can be observed in Figure S5. Even after the incorporation of PVDF, the absorbance spectra matched those of pure quasi-2D perovskites. A slight decrease in the onset sharpness (~550 nm) can be seen as a result of the scattering effect due to the presence of the PVDF matrix and the change in crystal size. Additional features of the absorbance can be seen at shorter wavelengths, which can be related to the perovskite dimensionality. Thus, the PVDF incorporation does not damage the optical properties of the perovskite.

Piezoelectricity derives from the polarization of material, creating an electric field that assists the charge formation and movement. Therefore, polarization has a direct impact on the piezoelectric coefficient, which is related to the dielectric permittivity (ε) and remnant polarization (P_r) by $d_{33} \propto \varepsilon P_r$. It is known that in the perovskite structure, the A-site cation is the main polarization origin, also related to the A-cation rotation degree of freedom. Another crucial parameter for the piezoelectric properties is the centro-symmetry of the crystal. In order to achieve the piezoelectric response, there is a requirement to break the centro-symmetry of the crystal and to form a noncentrosymmetric structure. In perovskite, the centro-symmetry derives from the BX_6 pyramids; therefore, the symmetry will break when the B cation moves away from the center of the octahedron. Our hypothesis is to break the symmetry by incorporating different sizes and lengths of A-site cations in the perovskite lattice. Since the A-site cation lays within the octahedral hole, the large size and irregular shape of the organic molecule lead to changes in the Br−Pb−Br bonds, resulting in enhanced centro-symmetry breaking of the BX_6 pyramid. We conducted a series of lateral and horizontal PFM measurements for each of the quasi-2D perovskite compositions to investigate the influence of the barrier molecule on the piezoelectric properties. Specific details of the measurement can be found in the Supporting Information (SI). In all

https://doi.org/10.1021/acsenergylett.4c00177
ACS Energy Lett. 2024, 9, 1527−1536

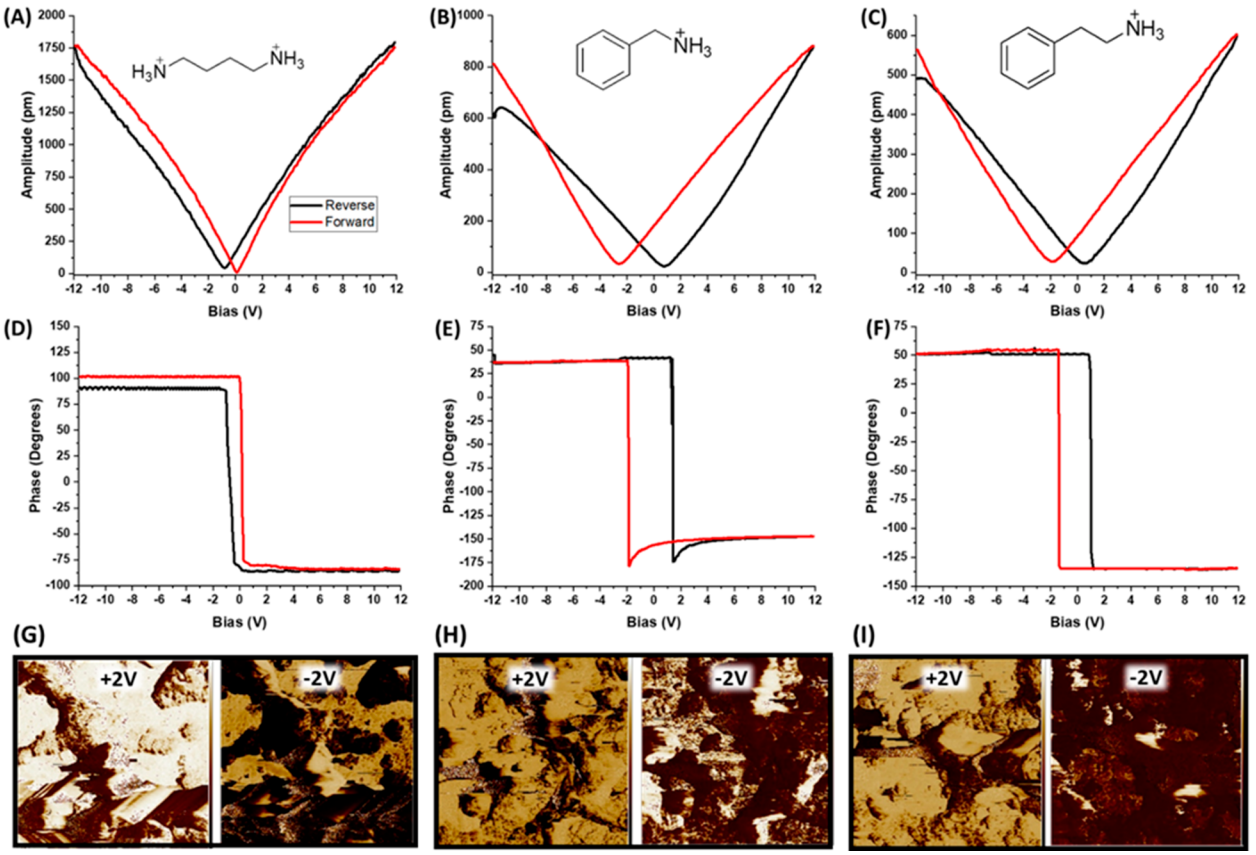

Figure 3. Local horizontal piezoelectric measurements for n = 5. The butterfly shape curves and corresponding phase curves of perovskites based on (A, D) BuDA, (B, E) BzA, and (C, F) PEA with 75% PVDF. The effect of polling (+2 V) and antipolling (−2 V) on (G) PEA-, (H) BzA-, and (I) BuDA-based perovskites.

samples, we scanned an area of 5 × 5 μm^2 and applied a bias in the range of ±12 V. Based on the PFM results, we plotted the butterfly shaped amplitude and phase curves for each quasi-2D perovskite film. We studied the same barrier molecules for the n = 1 2D perovskites, n = 5, n = 10, and n = 50. Importantly, in the case of n = 1, the MA cation is not present and the perovskite structure only contains the barrier molecules.

Figure 2A−C show the "butterfly" shape curves measured by horizontal PFM for n = 1 quasi-2D perovskites based on BuDA, BzA, and PEA, respectively. From the "butterfly" curves, it can be seen that the distance between the two minimum points of the forward and backward scans is negligible and results in values of 0.47, 0.28, and 0.83 V, respectively. The minimum points of each graph show the voltages in which the dipoles changed their direction, while the distances between the two minimum points indicate the tolerance of the dipoles to change their orientation under the applied external electric field in the opposite direction. The fact that the dipoles in the case of n = 1 cannot resist the opposite field indicates piezoelectric response.

The amplitude of the curve is the maximum point at which the two curves overlap. The value of this parameter shows the magnitude of the piezoelectric response in terms of material contraction as a result of the applied external field since it is proportional to the effective piezoelectric constant of the material. The extracted amplitude values of n = 1 BuDA, BzA, and PEA compositions were 1021, 418, and 419 pm, respectively.

Figure 2D−F present the corresponding phase curves with respect to the applied bias for BuDA, BzA, and PEA, respectively. All three curves demonstrate a clear 180° switching that indicates the polarization swap upward or downward according to the external electric field direction. The PFM phase is the phase lag between the applied bias on the probe and the strain response which is measured. It provides information on the direction of the polarization. The observed trends from different compositions can be explained by different values of the molecular polarizabilities of the barrier (α) since they are defined as the ability to become polarized by an electric field, i.e., P = αE.

In addition to the piezoelectricity along the horizontal direction, we measured the response along the lateral direction for each composition. Both butterfly and the corresponding phase curves are presented in Figure S6. We observed a similar trend as in the case of the horizontal measurements in which BuDA demonstrated the highest piezoelectric response of 4 mV, followed by BzA with an amplitude of 1.7 and 1.2 mV for PEA-based composition. However, in terms of the ability to maintain the dipole direction under an applied external field, the opposite trend can be seen where the distances between the two minimum points were 0.27 1.85, and 3.95 V for BuDA, BzA, and PEA-based 2D perovskites, respectively.

Next, we synthesized n = 5 quasi-2D perovskite using the same barrier molecules, which include the MA^+ cation in the lattice. Figure 3A−C present the butterfly curves for n = 5 BuDA-, BzA-, and PEA-based perovskites, respectively. In comparison to the PFM measurements of the n = 1

https://doi.org/10.1021/acsenergylett.4c00177
ACS Energy Lett. 2024, 9, 1527−1536

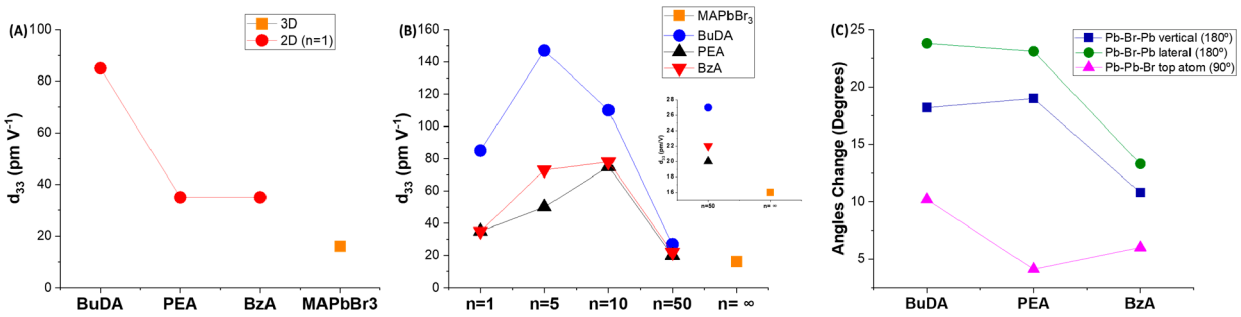

Figure 4. (A) d_{33} values of pure 2D perovskites (n = 1) compare to the corresponding 3D perovskite. (B) d_{33} values as a function of the "n" value and n = ∞ for 3D $MAPbBr_3$. The barrier molecules: BuDA (blue), PEA (black), and BzA (red), the inset shows a magnification of the n = 50 and ∞ region. (C) The change in the octahedrons bond angles under a pressure of 0.5 MPa for the different barrier molecules calculated by DFT.

compositions, it can be seen that for n = 5, the distance between the two minimum points of the curves is larger with increased values of 2.36 3.34, and 0.88 V, while the amplitude values were 602, 881, and 1761 pm for PEA, BzA, and BuDA, respectively. Figure 3D–F show the corresponding phase curves for the quasi-2D n = 5 perovskite compositions based on the above three barrier molecules. The phase curves showed 180° switching in polarization for all the studied quasi-2D perovskites. All three curves show a change of the dipole orientation as a function of the applied bias. However, it can be seen that the curves minimum points are not symmetric along the bias axis and tend to be in the negative bias region. This can be attributed to the initial inner dipole moment which exists in the perovskite. In other words, it indicates the existence of spontaneous dipole orientation within the material even without an external electric field. The lateral piezoelectric response was also measured for the n = 5 compositions, as can be seen in Figure S7. Similarly, as in the case of the horizontal response, a significant increase in the amplitudes, with respect to the compounds with n = 1, was observed and yielded values of 40.7, 21.3, and 40.4 mV for BuDA, BzA, and PEA, respectively. We also observed an increase in the distances between the curve's minimum points, namely 1.06, 4.22, and 4.03 V for BuDA, BzA, and PEA compositions, respectively. Hence, the quasi-2D n = 5 compositions undergo a more significant structural change in response to the external field than the n = 1 cases with the corresponding barrier molecules. Additionally, Figure 3G–I present the phase scanning images under positive (+2 V) and negative (−2 V) bias to demonstrate the polling effect for PEA, BzA and BuDA, respectively. Upon polling, it can be seen that the piezoelectric domains of all three compositions flip their conductivity according to the direction of the applied external field.

BuDA forms a DJ structure in which the spacing between the octahedral sheets is smaller compared to the RP structures that are formed by the BzA and PEA barriers. In terms of molecular length, BuDA has a size of 9.37 Å, similar to PEA with a size of 9.46 Å, which is longer compared to the BzA molecule (7.83 Å). On the other hand, BuDA is a linear molecule without the bulky phenyl ring that would aggregate with neighboring barrier molecules. Therefore, this molecule penetrates more deeply into the perovskite, breaking the centro-symmetry more significantly than it is in the case of other barrier molecules. As a result, the distortions of the perovskite geometry are responsible for the enhanced piezoelectric response in the case of BuDA as the molecule barrier.

To investigate further the effect of MA dipoles and to evaluate the impact of the barrier molecules on the piezoelectric properties, we performed the same measurements on pure (no barrier molecules) $MAPbBr_3$:PVDF composite film. Previous reports showed that 3D MA-based perovskite has a piezoelectric response.[33,34,23] However, the piezoelectric coefficient does not have a fixed absolute value, and it is expected to vary as a function of the fabrication process and layer quality. Figure S8A and B show the horizontal and vertical butterfly curves that were obtained from PFM, respectively. The corresponding phase curves are presented in Figure S8D and E along with phase images under negative and positive biases of ±2 V (Figure S8C and F). $MAPbBr_3$:PVDF composite films show a piezoelectric response, as expected with similar butterfly and phase curves. However, it can be seen that the piezoelectric response of $MAPbBr_3$ is weaker compared to the quasi-2D based perovskites; it results in a lower amplitude of ∼185 pm and 3.8 mV for the horizontal and vertical measurements, respectively. Based on the amplitude values, the piezoelectric coefficient (d_{33}) for each composition can be calculated. In the case of n = 1, we observed a d_{33} value of 85 pm V^{-1} for the BuDA-based composition and for BzA and PEA, the same piezoelectric coefficient was observed of 35 pm V^{-1}. Those experimental values are higher compared to previous works which were conducted for 3D perovskites such as $MASnI_3$ (20.8 pm V^{-1}), $FAPbBr_3$ (25 pm V^{-1}), and $MAPbI_3$ (25 pm V^{-1}).[29,35,36] The calculated d_{33} value for the 3D composition was 15.4 pm V^{-1}, which is significantly lower compared to all low dimensional compositions (Figure 4B), which emphasized the contribution of the barrier molecules to the enhancement of the piezoelectric response in perovskite. The enhancement in the d_{33} values of the 2D perovskites compared to the 3D perovskite can be seen in Figure 4A. An additional enhancement of the d_{33} values in the case of n = 5 compared to n = 1 compositions that were extracted from the corresponding amplitudes was also observed which resulted with 50 pm V^{-1}, 73 pm V^{-1}, and 147 pm V^{-1} for PEA-, BzA-, and BuDA-based perovskite, respectively. The reason for the enhanced piezoelectric response in the case of n = 5 is the presence of a larger proportion of the MA cation which contributes to the piezoelectric effect in two ways; (i) MA cation has a strong dipole of 2.29D which assists in the charge transfer process and (ii) the size differences between the relatively small MA cation (1.8 Å) to the bulkier barrier molecule results in breaking the centro-symmetry of the crystal.[37,5]

https://doi.org/10.1021/acsenergylett.4c00177
ACS Energy Lett. 2024, 9, 1527−1536

An additional explanation is due to the thickness of the perovskite layer, which is derived from the barrier length. Increased perovskite layer thickness causes a larger contribution to the piezoelectric response that originates from the aforementioned breaking of the centro-symmetry of the PbX_6 pyramids. In such a mechanism, the barrier molecules would act only as "hammers" that propagate the compressive forces deeply into the compound. Taking a closer look into the perovskite symmetry breaking, we notice that barrier molecules occupy the octahedral holes of the quasi-2D perovskite surface deeply or shallower, depending on their van der Waals volume (V_{vdW}). Comparison of the barrier molecules in terms of the V_{vdW} is preferential for BuDA with its smallest V_{vdW} of 79.08 $Å^3$, which deeply penetrates the perovskite causing its symmetry breaking. Between the two aromatic barriers, PEA has a larger V_{VDW} of 108.1 $Å^3$ in comparison to BzA with a V_{vdW} of 94.1 $Å^3$. Due to the larger volume, PEA occupies a larger space between the perovskite layers. PEA also enters the octahedral hole more deeply due to the larger residue (additional CH_2 segment); thus, we expect more significant distortions of the apical halide atoms and Pb−Br−Pb angles at the perovskite surface than would be in the case of BzA.

To further investigate the dimensionality impact on the piezoelectric coefficient, we synthesized higher "*n*" values (n = 10 and n = 50) based on each composition. Figures S9 and S10 present the butterfly curves and phase curves for n = 10 and n = 50, respectively. Based on these curves, the piezoelectric coefficients were extracted. Figure 4B presents the piezoelectric coefficients for BuDA, PEA, and BzA compositions as a function of the "*n*" value, where n = 1, 5, 10, 50, and ∞ (3D). In the case of PEA and BzA, we observed a small increase in the piezoelectric coefficient to 75 and 78 pm V^{-1}, respectively, for n = 10. However, for n = 10 based on BuDA, the piezoelectric coefficient reduces to a value of 110 pm V^{-1} compared to more than 140 pm V^{-1} for n = 5. The reason might be due to the fact that BuDA forms a DJ 2D structure where there is only one molecule that functions as a barrier between the octahedrons; therefore, there are fewer barrier molecules in the crystal structure compared to BzA and PEA 2D structures in which two barrier molecules form the RP 2D structure. As a result of the reduced amount of barrier molecules, a lower d_{33} value is observed for n = 10 compared to n = 5 in the case of BuDA. This explanation is supported by the decrease of d_{33} values for all compositions in the case of n = 50. As can be seen at the inset of Figure 4B, when n = 50, the d_{33} values become closer to those of the 3D perovskite having values of 20, 22, and 27 pm V^{-1} for PEA, BzA, and BuDA, respectively. Since the n = 50 composition contains a very small amount of barrier molecules, the system is very similar to the 3D perovskite, and therefore, its piezoelectric response is lower than that of the 2D (n = 1, n = 5, n = 10) perovskites. It can be noted that for all "*n*" values the BuDA compositions demonstrate the highest piezoelectric coefficient values.

For the sake of atomistic and electronic insight, we performed DFT calculations for the quasi-2D perovskite used in this work. The origin of polarization is in the polarizability of the whole system and the molecular and inorganic components. The inorganic frame contributes to this effect via breaking of the centro-symmetry of the $PbBr_6$ pyramids, while the molecular geometry also might change under pressure. Therefore, we optimized the atomic positions in the supercells that contain the quasi-2D $MAPbBr_3$ with three barrier molecules, PEA, BzA, and BuDA.

We extended the system laterally by the 2 × 2 × 1 repetition of the unit cell and randomly rotated the methylammunium molecules. Our calculations started with a little distorted $PbBr_6$ pyramids and the barrier molecules with geometries optimized in a vacuum. We placed the barriers between the perovskite layers in such a way that the phenyl rings of neighboring molecules were perpendicular. Thus, the interaction between the perovskite and barrier layer is weak; we named this setup "start". Further, we optimized the structures by applying the uniaxial pressure (along the *c*-axis of the compounds) choosing two values, 0.5 MPa (called "P1") and 2 MPa (called "P2"). Table S1 collects the maximal distortions, distances, and angles in the optimized structures under the assumed pressures and compared to the starting geometries with the imposed weak symmetry breaking. Figure 4C shows the changes in the bond angles for each composition under a pressure of 0.5 MPa (P1). The calculated distortions indicate that the applied uniaxial pressures push BuDA molecules inside the Pb−Br squares of the perovskite and do not change much the shape of this barrier. Pressures P1 and P2 lead to quite similar results for the barrier molecules because the top halide ions (that are placed on the *c*-axis in the Dion-Jacobson structure) prevent too strong shortening of the distance between the perovskite layers. For the same reason, the effect of applied pressure moves into the perovskite and results in the largest deformations of the $PbBr_6$ pyramids among all cases with barriers. This is manifested by a change of the Pb−Br−Pb angles and displacements of the top halides (Br−Pb−Pb angles). On the other hand, the largest effect of pressure in the barrier molecules is for PEA, in the place where the chain residue is attached to the phenyl ring (C−C−C angle). Since PEA is the most "bulky" molecule in its volume, the uniaxial compression should not push its $-NH_3$ group too deeply into the perovskite. On the other hand, the chain residue in PEA is longer than in BzA, thus enlarging its penetration ability with respect to the latter barrier. We see that in this case the effect of pressure in the crystal layer shows up in large distortions of the $PbBr_6$ pyramids.

To summarize, the effect of pressure acts mainly on the inorganic perovskite framework when the BuDA barrier is used, moderately in the case of the BzA on the inorganic perovskite framework and the barrier, and strongly on both components when PEA is used. All of the above-described distortions might cause a change in the polarizability in the studied 2D perovskites. The polarizability of a molecule, 2D or quasi-2D and 3D systems should be calculated according to different formulas. The 2D systems lack periodicity in the direction across the structure; thus, we can use the formula:

$$\epsilon^{\perp}(\mathbf{q}, \omega) = (1 - 2\pi\alpha^{\perp}(\omega)|\mathbf{q}|)^{-1}$$

for the perpendicular component. In contrast, our systems are periodic in all Cartesian coordinates, although the interaction between the perovskite and molecular layers is much weaker than that in the bulk. Therefore, in the quasi-2D systems, the polarizability α and the macroscopic dielectric function $\epsilon(\mathbf{q},\omega)$, where q is a wave vector in the first Brillouin zone (BZ) and $|\mathbf{q}|$ is its module while ω is a frequency, are related by the two simple expressions:[38,39]

$$\epsilon^{\parallel}(\mathbf{q}, \omega) = 1 + 2\pi\alpha^{\parallel}(\omega)|\mathbf{q}| \quad \text{for the in-plane component}$$

https://doi.org/10.1021/acsenergylett.4c00177
ACS Energy Lett. 2024, 9, 1527−1536

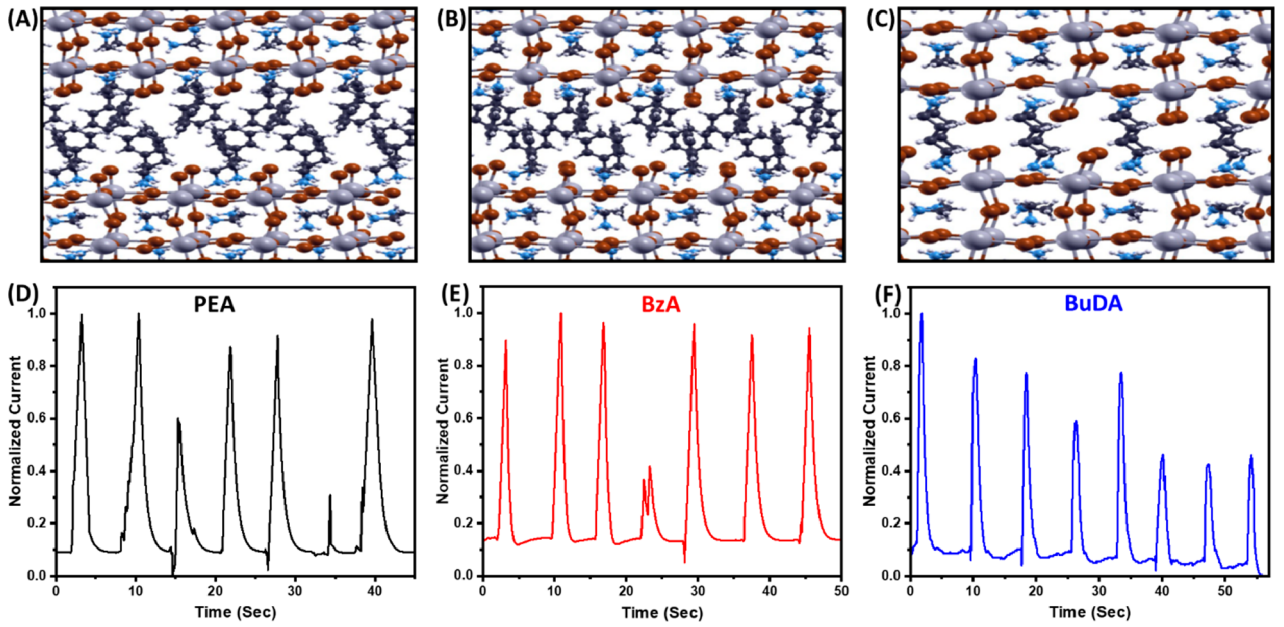

Figure 5. (A–C) The quasi-2D structures of $MAPbBr_3$ with PEA, BzA, and BuDA were optimized with DFT for the uniaxial pressure of 0.5 MPa. Colors of the atoms: Pb, gray; Br, brown; C, black; N, blue; H, white. Normalized capacitance measurements for pressure sensors based on (D) PEA, (E) BzA, and (F) BuDA perovskites where n = 5.

$$\epsilon^{\perp}(\mathbf{q}, \omega) = 1 + 2\pi\alpha^{\perp}(\omega)|\mathbf{q}|$$

across the sandwich structure

With the *ai*-MBPT approach, we obtained the polarizabilities of quasi-2D $MAPbBr_3$ with three barrier molecules: BuDA, BzA, and PEA and at 0.5 MPa (systems can be seen in Figure 5A–C). In order to take into account a disorder of molecular orientations, for MA and barrier molecules, we performed the calculations using the supercells 2 × 2 × 1.

The values of the in-plane and out-of-plane polarizabilities ($\alpha^{\parallel}$ and $\alpha^{\perp}$) at zero frequency ($\omega = 0$) and the corresponding dielectric constants ($\epsilon^{\parallel}$ and $\epsilon^{\perp}$) are presented in Table 1. Full energy-resolved curves are presented in Figure S11. The largest dielectric constant and polarizability was calculated for quasi-2D perovskite with BuDA, which is in good agreement with the experimental results, and also supports the origin of the high piezoelectric response recorded by the PFM measurements. For a comparison, we also added to Table 1 the results for bulk (3D) $MAPbBr_3$ under pressure and 2D case (n = 3) terminated with MA. These cases were also calculated in the supercells 2 × 2 × 1 including the disorder. We derive the conclusion that the perovskite materials with disordered MA cations (rows 4 and 5 in Table 1) show lower polarizabilities than the case with the MA molecules aligned in the same direction, in agreement with our experimental results. It is important to note that we do not know the direction of MA dipoles which was assumed in previous work.[38] Also, the effect of pressure in the 3D case has a strong impact on polarizability with respect to much less distorted 2D without compression.

Table 1. Macroscopic Dielectric Constant (Relative to ε_0) and Polarizability (in Å/ε_0), for the in-Plane and out-of-Plane Components, Were Obtained for the Studied Systems with the *Ab Initio* RPA Method[a]

	$\epsilon^{\parallel}(\mathbf{q}, \omega = 0)$	$\alpha^{\parallel}(\omega = 0)$	$\lvert\mathbf{q}\rvert$	$\epsilon^{\perp}(\mathbf{q}, \omega = 0)$	$\alpha^{\perp}(\omega = 0)$	$\lvert\mathbf{q}\rvert$
$MAPbBr_3$ (PEA), ⊥0.5 MPa	7.21	3.74	0.042	26.97	35.85	0.018
$MAPbBr_3$ (BzA), ⊥0.5 MPa	7.11	3.68	0.042	22.28	26.97	0.020
$MAPbBr_3$ (BuDA), ⊥0.5 MPa	19.98	11.42	0.042	55.58	57.43	0.024
$MAPbBr_3$ (2D)[b]	1.88	0.38	0.060	5.63	1.25	0.017
$MAPbBr_3$ bulk (30), ⊥0.5 MPa[b]	11.09	4.29	0.060	16.88	8.83	0.046
MAPbBr3 n = 1 (2D)[c]		~15.7			~8.0	

[a]The module of the chosen **q**-point in BZ is in the units of 2π/Å. [b]Disorder of MA was simulated in the 2 × 2 × 1 supercell. [c]Estimated from Figure 2 where the authors obtained them with the *ab initio* BSE method for the system without the disorder of MA orientations.[38]

The above numerical results lead to 2-fold conclusions. (1) Distortions of perovskite and disorder of molecular dipoles make a very strong impact on the piezoelectric properties, and these effects are opposed to each other (the former increases and the latter decreases the polarizability), while the effect of pressure enlarges the effect of distortions. We oriented the phenyl rings of the neighboring barrier molecules (for PEA and BzA cases) perpendicular to each other, and this fact might weaken the effect of the dipole orientations on the total polarizability of the system. On the other hand, four BuDA molecules (being the linear barriers) were aligned very regularly in the 2 × 2 × 1 supercells. This fact, in turn, might lead to an accumulation of the crystal distortions, which would only increase the total polarizability of the supercell. Much larger supercells with BuDA, and the introduction of the molecular tilting disorder (not taken into account in our simulations), certainly would distort the $PbBr_6$ pyramids of perovskite layers less "homogeneously" and cause a decrease of the polarizabilities. (2) In our simulation, we did not take into account the effect of the PVDF medium and the charge

https://doi.org/10.1021/acsenergylett.4c00177
ACS Energy Lett. 2024, 9, 1527–1536

transfer effects. One should be made of the electronic potential barriers at the interfaces between PVDF and the perovskite for electron states and hole states. Moreover, the molecular crystals exhibit hopping conductivity; thus, the charge transfer from the barrier molecules to the PVDF might also be not negligible.

In order to observe the piezoelectric properties on the macroscopic scale, we fabricated pressure sensor devices. The pressure sensor structure is fabricated by the deposition of perovskite:PVDF composite film on top of an ITO-coated PET substrate followed by a layer of polydimethylsiloxane (PDMS), which forms the bottom contact. Next, Au-coated PET is attached on top of the bottom part by curing PDMS between the two parts. Upon applied pressure, the dipoles within the perovskite start to organize in a preferred orientation directing the electrons and holes toward the contacts. Figure 5A−C show the calculated distortions of the bond angles as a result of an external pressure of 0.5 MPa for PEA-, BzA-, and BuDA-based perovskites, respectively. We incorporated each 2D perovskite composition (n = 5) as the active layer in the pressure sensor and measured the capacitance response to finger tapping. The device capacitance measurements for PEA-, BzA-, and BuDA-based perovskites are presented in Figure 5D−F, respectively. It can be seen that in the case of the two aromatic molecules (PEA and BzA) the amount of separated charge (the peak maxima) maintains ∼90% of its initial value with each finger tapping. The decay time of each sensor was calculated based on the capacitance measurements and found to be 0.637 ± 0.010, 0.574 ± 0.016, and 0.649 ± 0.064 s for PEA, BuDA, and BzA, respectively. On the other hand, the BuDA-based sensor shows a decrease in the generated current values with each press during time. The reason for this decrease in piezoelectricity is a fingerprint of the damage to the homogeneous alignment of the barrier molecules. In other words, by applying pressure, the molecular tilting changes with respect to the perovskite planes and the resulting perovskite distortions become irregular. In contrast, the aromatic barriers are more resistant to such damage due to their more densely packed structure in quasi-2D perovskites and stronger electronic interactions between the phenyl rings that prevent changes in the geometry. The capacitance decay time of the pressure sensors shows that the PEA-based device can maintain the separated charges for a longer time compared to the BzA-based device.

In this work, the effect of the barrier molecule type and dimensionality in hybrid perovskite on the piezoelectric properties was investigated. Three barrier molecules, BuDA, BzA, and PEA, were studied for both n = 1 and n = 5 compositions. When mixing these quasi-2D perovskites with PVDF, the preferred crystal orientation and size were changed. A series of both lateral and horizontal PFM measurements demonstrate that BuDA-based composition has the highest piezoelectric response which results in a piezoelectric coefficient (d_{33}) of 85 pm V^{-1} compared to 35 pm V^{-1} for the two aromatic barrier molecules. DFT calculations showed that BuDA causes a much more significant distortion in the bond angles of the $PbBr_6$ pyramids due to its smaller size that allows deeper penetration within the perovskite, leading to enhanced symmetry breaking which contributes to the piezoelectric effect. Furthermore, the *ai*-MBPT calculations of the polarizabilities and the corresponding dielectric constants in both horizontal and lateral directions yielded the highest values for BuDA, followed by those for PEA and BzA, further supporting our experimental results. Clearly when increasing the dimensionality to n = 5, the piezoelectric coefficient is increased mainly due to the incorporation of MA cations along with the barrier molecules that enhance the symmetry breaking. The quasi-2D perovskite (n = 5) resulted in enhanced piezoelectric coefficient values of 147 pm V^{-1}, 73 pm V^{-1}, and 50 pm V^{-1} for BuDA, BzA, and PEA, respectively. Finally, we fabricated a pressure sensor based on each quasi-2D perovskite. Such sensors can be used in a variety of applications, including soft robotics and wearable electronics. We revealed a faster decay time of the BuDA-based sensor in comparison to the aromatic-barriers-based sensors. However, due to the damage of the homogeneous alignment of the barrier molecules, the BuDA-based sensors could not maintain the same amount of charge generated each time.

■ ASSOCIATED CONTENT

Supporting Information

The Supporting Information is available free of charge at https://pubs.acs.org/doi/10.1021/acsenergylett.4c00177.

Experimental details, materials, and characterizations including SC-XRD data, absorbance measurements, SEM images, and additional PFM curves; full energy curves for 3D, 2D, and quasi-2D $MAPbBr_3$; table with calculated values of bond distortions (PDF)

■ AUTHOR INFORMATION

Corresponding Author

Lioz Etgar − *Institute of Chemistry, The Center for Nanoscience and Nanotechnology, Casali Center for Applied Chemistry, The Hebrew University of Jerusalem, Jerusalem 91904, Israel; The Smart Grippers for Soft Robotics (SGSR) Program, Campus for Research Excellence and Technological Enterprise (CREATE), Singapore-HUJ Alliance for Research and Enterprise, 138602, Singapore;* orcid.org/0000-0001-6158-8520; Email: lioz.etgar@mail.huji.ac.il

Authors

Stav Rahmany − *Institute of Chemistry, The Center for Nanoscience and Nanotechnology, Casali Center for Applied Chemistry, The Hebrew University of Jerusalem, Jerusalem 91904, Israel*

Adva Shpatz Dayan − *Institute of Chemistry, The Center for Nanoscience and Nanotechnology, Casali Center for Applied Chemistry, The Hebrew University of Jerusalem, Jerusalem 91904, Israel*

Małgorzata Wierzbowska − *Institute of High Pressure Physics Polish Academy of Sciences, 01-142 Warsaw, Poland;* orcid.org/0000-0002-4826-7076

Amanda Jiamin Ong − *School of Material Science and Engineering, Nanyang Technological University, 639798, Singapore; The Smart Grippers for Soft Robotics (SGSR) Program, Campus for Research Excellence and Technological Enterprise (CREATE), Singapore-HUJ Alliance for Research and Enterprise, 138602, Singapore;* orcid.org/0000-0001-9263-2387

Yun Li − *School of Material Science and Engineering, Nanyang Technological University, 639798, Singapore; The Smart Grippers for Soft Robotics (SGSR) Program, Campus for Research Excellence and Technological Enterprise (CREATE), Singapore-HUJ Alliance for Research and*

https://doi.org/10.1021/acsenergylett.4c00177
ACS Energy Lett. 2024, 9, 1527−1536

Enterprise, 138602, Singapore; orcid.org/0000-0001-7349-5209

Shlomo Magdassi − *Institute of Chemistry, The Center for Nanoscience and Nanotechnology, Casali Center for Applied Chemistry, The Hebrew University of Jerusalem, Jerusalem 91904, Israel; The Smart Grippers for Soft Robotics (SGSR) Program, Campus for Research Excellence and Technological Enterprise (CREATE), Singapore-HUJ Alliance for Research and Enterprise, 138602, Singapore;* orcid.org/0000-0002-6794-0553

Alfred Iing Yoong Tok − *School of Material Science and Engineering, Nanyang Technological University, 639798, Singapore; The Smart Grippers for Soft Robotics (SGSR) Program, Campus for Research Excellence and Technological Enterprise (CREATE), Singapore-HUJ Alliance for Research and Enterprise, 138602, Singapore;* orcid.org/0000-0003-3546-7180

Complete contact information is available at: https://pubs.acs.org/10.1021/acsenergylett.4c00177

Notes

The authors declare no competing financial interest.

■ ACKNOWLEDGMENTS

This research was supported by grants from the National Research Foundation, Prime Minister's Office, Singapore under its Campus of Research Excellence and Technological Enterprise (CREATE) program and by the Air Force Research Laboratory (AFRL). The calculations have been supported by the National Science Centre of Poland, grant no. 2019/33/B/ST8/02105. We gratefully acknowledge Polish high-performance computing infrastructure PLGrid (ACK Cyfronet AGH) for providing computer facilities and support within computational grant no. PLG/701 2023/016743.

■ REFERENCES

(1) Mitzi, D. B. Synthesis, structure, and properties of organic-inorganic perovskites and related materials. *Prog. Inorg. Chem.* **2007**, *48*, 1−121, DOI: 10.1002/9780470166499.ch1.

(2) Yin, W. J.; Yang, J. H.; Kang, J.; Yan, Y.; Wei, S. H. Halide perovskite materials for solar cells: A theoretical review. *J. Mater. Chem. A* **2015**, *3*, 8926−8942.

(3) Chang, Y. H.; Park, C. H.; Matsuishi, K. First-Principles Study of the Structural and the Electronic Properties of the Lead-Halide. *J. Korean Phys. Soc.* **2004**, *44*, 889−893.

(4) Qiu, L.; He, S.; Ono, L. K.; Qi, Y. Progress of Surface Science Studies on ABX3-Based Metal Halide Perovskite Solar Cells. *Adv. Energy Mater.* **2020**, *10*, 1902726.

(5) Li, C.; et al. Formability of ABX 3 (X = F, Cl, Br, I) halide perovskites. *Acta Crystallogr. Sect. B Struct. Sci.* **2008**, *64*, 702−707.

(6) Park, N. G. Perovskite solar cells: An emerging photovoltaic technology. *Mater. Today* **2015**, *18*, 65−72.

(7) Travis, W.; Glover, E. N. K.; Bronstein, H.; Scanlon, D. O.; Palgrave, R. G. On the application of the tolerance factor to inorganic and hybrid halide perovskites: A revised system. *Chem. Sci.* **2016**, *7*, 4548−4556.

(8) Li, Z.; et al. Stabilizing Perovskite Structures by Tuning Tolerance Factor: Formation of Formamidinium and Cesium Lead Iodide Solid-State Alloys. *Chem. Mater.* **2016**, *28*, 284−292.

(9) Kieslich, G.; Sun, S.; Cheetham, A. K. An extended Tolerance Factor approach for organic-inorganic perovskites. *Chem. Sci.* **2015**, *6*, 3430−3433.

(10) Saliba, M.; et al. Incorporation of rubidium cations into perovskite solar cells improves photovoltaic performance. *Science* **2016**, *354*, 206−209.

(11) Zhang, L.; Liu, Y.; Yang, Z.; Liu, S. Two dimensional metal halide perovskites: Promising candidates for light-emitting diodes. *Journal of Energy Chemistry* **2019**, *37*, 97−110.

(12) Cohen, B. El; Li, Y.; Meng, Q.; Etgar, L. Dion-Jacobson Two-Dimensional Perovskite Solar Cells Based on Benzene Dimethanammonium Cation. *Nano Lett.* **2019**, *19*, 2588−2597.

(13) Mao, L.; et al. Hybrid Dion-Jacobson 2D Lead Iodide Perovskites. *J. Am. Chem. Soc.* **2018**, *140*, 3775−3783.

(14) Chen, Y.; et al. 2D Ruddlesden−Popper Perovskites for Optoelectronics. *Adv. Mater.* **2018**, *30*, 1703487.

(15) Shpatz Dayan, A.; et al. Enhancing Stability and Photostability of CsPbI3 by Reducing Its Dimensionality. *Chem. Mater.* **2018**, *30*, 8017−8024.

(16) Ma, C.; et al. 2D/3D perovskite hybrids as moisture-tolerant and efficient light absorbers for solar cells. *Nanoscale* **2016**, *8*, 18309−18314.

(17) Sutanto, A. A.; et al. In Situ Analysis Reveals the Role of 2D Perovskite in Preventing Thermal-Induced Degradation in 2D/3D Perovskite Interfaces. *Nano Lett.* **2020**, *20*, 3992−3998.

(18) Zheng, T.; Wu, J.; Xiao, D.; Zhu, J. Recent development in lead-free perovskite piezoelectric bulk materials. *Prog. Mater. Sci.* **2018**, *98*, 552−624.

(19) Li, F.; et al. Piezoelectric activity in perovskite ferroelectric crystals. *IEEE Trans. Ultrason. Ferroelectr. Freq. Control* **2015**, *62*, 18−32.

(20) Jella, V. A comprehensive review of flexible piezoelectric generators based on organic-inorganic metal halide perovskites. *Nano Energy* **2019**, *57*, 74−93.

(21) Zhao, Y. Q.; Ma, Q. R.; Liu, B.; Yu, Z. L.; Cai, M. Q. Pressure-induced strong ferroelectric polarization in tetra-phase perovskite CsPbBr3. *Phys. Chem. Chem. Phys.* **2018**, *20*, 14718−14724.

(22) Ding, R.; Zhang, X.; Sun, X. W. Organometal Trihalide Perovskites with Intriguing Ferroelectric and Piezoelectric Properties. *Adv. Funct. Mater.* **2017**, *27*, No. 1702207.

(23) Jella, V.; Ippili, S.; Eom, J. H.; Choi, J.; Yoon, S. G. Enhanced output performance of a flexible piezoelectric energy harvester based on stable MAPbI3-PVDF composite films. *Nano Energy* **2018**, *53*, 46−56.

(24) Qin, Y.; et al. Multifunctional Chiral 2D Lead Halide Perovskites with Circularly Polarized Photoluminescence and Piezoelectric Energy Harvesting Properties. *ACS Nano* **2022**, *16*, 3221−3230.

(25) Jiang, W.; Zhang, R.; Jiang, B.; Cao, W. Characterization of piezoelectric materials with large piezoelectric and electromechanical coupling coefficients. *Ultrasonics* **2003**, *41*, 55−63.

(26) Nguyen, T. M. T.; et al. Enhanced Output Performance of Nanogenerator Based on Composite of Poly Vinyl Fluoride (PVDF) and Zn:Al Layered-Double Hydroxides (LDHs) Nanosheets. *Trans. Electr. Electron. Mater.* **2018**, *19*, 403−411.

(27) Lu, L.; Ding, W.; Liu, J.; Yang, B. Flexible PVDF based piezoelectric nanogenerators. *Nano Energy* **2020**, *78*, No. 105251.

(28) Ippili, S.; Jella, V.; Kim, J.; Hong, S.; Yoon, S. G. Unveiling Predominant Air-Stable Organotin Bromide Perovskite toward Mechanical Energy Harvesting. *ACS Appl. Mater. Interfaces* **2020**, *12*, 16469−16480.

(29) Han, B.; et al. High output piezoelectric composite nanogenerators composed of FAPbBr3-PVDF. *Conference Program Digest - 7th International Conference on Manipulation, Manufacturing and Measurement on the Nanoscale, IEEE 3M-NANO 2017*; IEEE, 2018; pp 371−374.

(30) Milot, R. L.; et al. Charge-Carrier Dynamics in 2D Hybrid Metal-Halide Perovskites. *Nano Lett.* **2016**, *16*, 7001−7007.

(31) Thrithamarassery Gangadharan, D.; Ma, D. Searching for stability at lower dimensions: current trends and future prospects of layered perovskite solar cells. *Energy Environ. Sci.* **2019**, *12*, 2860−2889.

(32) Cohen, B. El; et al. Hydroxyl Functional Groups in Two-Dimensional Dion-Jacobson Perovskite Solar Cells. *ACS Energy Lett.* **2022**, *7*, 217−225.

(33) Paul, T.; et al. Cube shaped FAPbBr3 for piezoelectric energy harvesting devices. *Mater. Lett.* **2021**, *301*, 130264.
(34) Lee, Y. H.; et al. Significant enhancement of the output voltage of piezoelectric/triboelectric hybrid nanogenerators based on MAPbBr3 single crystals embedded into a porous PVDF matrix. *Nano Energy* **2022**, *102*, 107676.
(35) Ippili, S.; et al. An eco-friendly flexible piezoelectric energy harvester that delivers high output performance is based on lead-free MASnI 3 films and MASnI 3 -PVDF composite films. *Nano Energy* **2019**, *57*, 911−923.
(36) Ding, R.; et al. Flexible Piezoelectric Nanocomposite Generators Based on Formamidinium Lead Halide Perovskite Nanoparticles. *Adv. Funct. Mater.* **2016**, *26*, 7708−7716.
(37) Frost, J. M.; et al. Atomistic origins of high-performance in hybrid halide perovskite solar cells. *Nano Lett.* **2014**, *14*, 2584−2590.
(38) Tian, T.; et al. Electronic Polarizability as the Fundamental Variable in the Dielectric Properties of Two-Dimensional Materials. *Nano Lett.* **2020**, *20*, 841−851.
(39) Thygesen, K. S. Calculating excitons, plasmons, and quasiparticles in 2D materials and van der Waals heterostructures. *2D Mater.* **2017**, *4*, No. 022004.

https://doi.org/10.1021/acsenergylett.4c00177
ACS Energy Lett. 2024, 9, 1527−1536